# Influence of $\pi$-Stacking on the Resonant Enhancement of the Second-Order Nonlinear Optical Response of Dipolar Chromophores

**Wei Zhang, Anthony F. Cozzolino, Amir H. Mahmoudkhani, Mark Tulumello, Sarah Mansour, and Ignacio Vargas-Baca***

*Department of Chemistry, McMaster University, 1280 Main Street West, Hamilton, Ontario L8S 4M1, Canada*

*Received: June 10, 2005; In Final Form: August 1, 2005*

The wavelength-dependent second-harmonic generation (SHG) efficiency of two simple dipolar chromophores, 4-$NO_2C_6H_4N(H)Bu^n$ (**1**) and 4-$NO_2C_6H_4SN(H)Bu^t$ (**2**), was compared in solution and in the solid state. Hyper-Rayleigh scattering measurements at 532 nm provided comparable molecular first hyperpolarizabilities. Both compounds crystallize in non-centrosymmetric space groups, but a more efficient arrangement of dipole moments results in a significantly larger $d_{eff}$ value for **2**. Kurtz−Perry experiments from 450 to 700 nm revealed an important difference in the resonant component of the nonlinear optical responses of these compounds; the SHG efficiency of crystalline **1** depends more strongly on the incident wavelength than that of **2**. This would be in contradiction with the TD-DFT excitation energies calculated for these molecules, but the observation can be explained by the resonant contribution from low-energy interchromophore excitations enabled by $\pi$-stacking in the crystal of **1**.

## Introduction

Comprehensive work carried out over the last three decades in organic nonlinear optics has led to a thorough understanding of the origins of molecular nonlinear responses.[1−6] Big dipole moments and a high degree of bond-length alternation are known to result in large first hyperpolarizabilities ($\beta$).[7−10] Alternative octupolar geometries have also been studied in detail.[11−15] These concepts have been extended to compounds of transition metals.[16−20] Recent investigations have been concerned with the experimental inability to reach the maximum hyperpolarizabilities allowed by quantum mechanics,[21−24] a limitation that recently was reported to be overcome by the third-order response of a fullerene polymer.[25] Important advances have also been achieved in the design of molecular and supramolecular non-centrosymmetric arrangements of nonlinear optical chromophores to enable macroscopic second-order effects.[26] Other strategies seek to correlate the responses of individual centers[27,28] or enhance the response in chiral media.[29−31]

Nonlinear optical crystal-lattice engineering has been conducted mostly under the premise that the overall response is the result of the sum of individual contributions of each molecule, the geometry of the arrangement being the main feature to tailor. The optimal orientation of dipolar chromophores in all non-centrosymmetric space groups has been calculated using such arguments.[32,33] These ideas have been extended to the octupolar case.[34] For simplicity, the effect of intermolecular interactions in the crystal is usually approximated. Dressed hyperpolarizabilities are corrected values obtained from considering the interaction of the chromophore with a polarizable continuous dielectric that mimics the immediate surroundings.[35] The application of such "dilute solute" models to the solid phase has proven useful not only for doped polymers but also for many organic nonlinear optical crystals. Investigations of molecular self-polarization as a function of interchromophore separation[36] have led to the design of very efficient nonlinear optical chromophores for polymer doping.[37] The effect of hydrogen bonding in solution has also been discussed.[38,39] In the solid, studying the effect of all the different types of intermolecular interactions on the nonlinear response is difficult because it is virtually impossible to control the organization of the chromophore in order to enable or disable selectively one particular interaction without introducing structural modifications that impact the electronic structure and the optical properties. However, the use of approximate models is valid in most cases because intermolecular interactions are 1 or 2 orders of magnitude smaller than intramolecular covalent bonds[40] and, in any case, their influence on electronic excitation processes should be minimal. A possible exception to this rule is the $\pi$-stacking interactions, despite being less than 50 kJ/mol, which enable through-space intramolecular charge transfers; this phenomenon has been used to design paracyclophanes with large hyperpolarizabilities.[41,42] In the intermolecular case, $\pi$-stacking can result in interchromophore excitations that will contribute to the resonant enhancement of the overall nonlinear response.

Here we report the use of second-harmonic generation at different wavelengths to compare the resonant contributions of two simple dipolar chromophores, nitroaniline (**1**) and nitrosulfenamide (**2**) (Chart 1). Their electronic structures are similar enough to yield comparable hyperpolarizabilities. Both compounds pack in non-centrosymmetric lattices; one is more efficient than the other for second-harmonic generation, but the most interesting difference in the crystal structures is that one compound exhibits strong $\pi$-stacking, the other does not. The $\pi$ intermolecular interaction does result in excitations that are observable in the linear absorption spectrum of **1** and thus could have an influence on the nonlinear response.

## Experimental Section

**Materials.** The manipulation of air-sensitive materials was performed under an atmosphere of dry argon or nitrogen with standard Schlenk and glovebox techniques. All solvents and reagents were dried and purified by standard procedures

* To whom correspondence should be addressed. Tel: 905 525 9140, ext 23497. Fax: 905 522 2509. E-mail: vargas@chemistry.mcmaster.ca.

10.1021/jp053142u CCC: $30.25 
Published on Web 09/10/2005

**CHART 1**

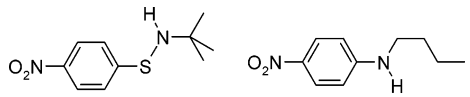

**1** **2**

immediately before use. The synthesis of compound **1** was carried out as published.[43] All other chemicals were used as received from Aldrich, Alfa Aesar, Fisher, or Caledon. HPLC-grade acetone was used for hyperpolarizability measurements in solution.

**Synthesis of 4-$NO_2C_6H_4S$-N(H)C$(CH_3)_3$ (2).** The disulfide $(4\text{-}NO_2C_6H_4S)_2$ (1.0011 g, 3.24 mmol) was dissolved in dichloromethane (40 mL). A solution of $SO_2Cl_2$ (0.48 mL, 0.80 g, 5.93 mmol) in the same solvent (10 mL) was added dropwise. The color of the mixture changed from yellow to green, brown, and finally to orange. Ten drops of pyridine were added to complete the reaction. The mixture was stirred continuously for approximately 15h. Dichloromethane and the remaining excess $SO_2Cl_2$ were removed under vacuum, leaving a yellow-orange solid, which was purified by reduced-pressure distillation. The product was dissolved in dry ether (40 mL) and added slowly to a solution of *tert*-butylamine (1.7 mL, 1.183 g, 16.2 mmol) in the same solvent (20 mL) using a cooling bath to maintain room temperature. The solvent was removed in vacuo leaving an orange solid. This was extracted with dichloromethane. An abundant amount of *tert*-butylamine hydrochloride was separated by filtration. The filtrate was concentrated to produce a viscous orange oil. After recrystallization from hexanes, pale yellow crystals of **2** were obtained. Yield: 0.3138 g, 21%. mp: 72 °C. $^1$H NMR (ppm, $CDCl_3$): $\delta$ 8.12 [d, 2H, $^3J$ = 11 Hz, $NO_2C_6H_4$-SN(H)C$(CH_3)_3$], 7.47 [d, 2H, $^3J$ = 11 Hz, $NO_2C_6H_4$SN(H)C-$(CH_3)_3$], 2.85 [s, 1H, $NO_2C_6H_4$−SN(*H*)C$(CH_3)_3$], 1.21 [s, 9H, $NO_2C_6H_4$SN(H)C(C*H*$_3)_3$]. $^{13}$C{$^1$H} NMR (ppm, $CDCl_3$): $\delta$ 123.85, 121.87, 77.80, 77.17 [$NO_2C_6H_4$SN(H)C$(CH_3)_3$], 76.53 [$NO_2C_6H_4$SN(H)*C*$(CH_3)_3$], 29.22 [$NO_2C_6H_4$SN(H)C(*C*H$_3)_3$]. LR EI-MS *m*/*z*: 226 ($M^+$), 211 ($M^+$− $CH_3$), 170 ($M^+$− H−$C_4H_9$), 154 ($M^+$− $NHC_4H_9$), 140 ($M^+$− N−$NHC_4H_9$), 108 ($M^+$− $NO_2$−$NHC_4H_9$). HR EI-TOFMS: calcd *m*/*z* for $C_{10}H_{14}N_2O_2S^+$ 226.0776, exp. 226.0779. IR (cm$^{-1}$): 3320 m, 2967 m, 2904 m, 1717 m, 1576 m, 1500 m, 1367 m, 1326 m, 1309 m, 1290 m, 1244 m, 1202 m, 739 m. Raman (cm$^{-1}$): 84.3, 99.4, 119.9, 158.6, 275.0, 493.9, 525.3, 536.8, 626.7, 724.3, 755.8, 851.8, 1004.5, 1082.0, 1109.6, 1316.2, 1328.7, 1373.6, 1506.5, 1579.1.

**Spectroscopic Instrumentation.** IR spectra were recorded using a Bio-Rad FTS-40 FT-IR spectrometer. Each spectrum was acquired from KBr pellets with a resolution of 8 cm$^{-1}$, and the background, which was simultaneously subtracted, was recorded prior to a spectral acquisition. FT Raman spectra were recorded at ambient temperature in sealed Pyrex melting point capillaries using a Bruker RFS 100 spectrometer equipped with a quartz beam splitter and a liquid nitrogen cooled Ge diode detector. The 1064 nm line of an Nd:YAG laser (350 mW maximum output) was used for excitation of the sample with a spot of ca. 0.2 mm at the sample using 10−300 mW of power, and the backscattered radiation was sampled. The actual usable Stokes range was 100−3500 cm$^{-1}$ with a spectral resolution of 2 cm$^{-1}$. The Fourier transformations were carried out by using a Blackman−Harris four-term apodization and a zero-filling factor of 4. The $^1$H and $^{13}$C{$^1$H} NMR spectra in solution were recorded on a Bruker Avance AV200 (200.13 MHz) or AV300 (300.13 MHz) spectrometer. Chemical shifts are reported in ppm and were referenced to the residual-proton and natural-abundance peak of $CDCl_3$ ($\delta$ 7.24, $^1$H NMR; $\delta$ 77.0, $^{13}$C NMR). Mass spectra were acquired at the McMaster Regional Centre for Mass Spectrometry using a micromass GCT (EI/CI time-of-flight mass spectrometer).

**X-ray Crystallography.** High-quality single crystals of **2** were grown by slow evaporation of a hexanes solution at room temperature. A pale yellow crystal (0.35 × 0.14 × 0.06 mm$^3$) was mounted on a glass fiber and stored under nitrogen until installed in the diffractometer. Data were collected on a P4 Bruker diffractometer upgraded with a Bruker SMART 1000 CCD detector and a rotating anode utilizing Mo K$\alpha$ radiation ($\lambda$ = 0.71073 Å, graphite monochromator) equipped with an Oxford cryosystem. A full sphere of reciprocal lattice was scanned by 0.36° steps in $\omega$ with a crystal-to-detector distance of 4.97 cm. A preliminary orientation matrix was obtained from the first frames using SMART.[44] The collected frames were integrated using the preliminary orientation matrixes which were updated every 100 frames. Final cell parameters were obtained by refinement on the positions of reflections with $I > 10\sigma(I)$ after integration of all the frames using SAINT.[44] The data were empirically corrected for absorption and other effects using SADABS.[45] The structure was solved by direct methods and refined by full-matrix least-squares method on all $F^2$ data using SHELXTL.[46] The (N−)H atom was located from a difference Fourier map, whereas the (C−)H atoms were placed at 0.95 or 0.98 Å from the pivot atoms with bond angles constrained to idealized geometry using the appropriate riding model and refined isotropically; $U_{iso}$ values are in the range of 0.026−0.080 Å$^2$. The non-H atoms were refined anisotropically. Analysis of the molecular structure determined by X-ray diffraction was assisted by comparison to related structures compiled in the Cambridge Structural Database (CSD).[47]

**Second-Harmonic Generation.** A multipurpose harmonic-light spectrometer was employed for these measurements. The light source consisted of an optical parametric oscillator (OPO) pumped by a Nd:YAG laser (Continuum Surelite II). Dichroic mirrors and a long-pass filter were used to separate the signal from the idler outputs; this system delivered IR pulses with a repetition frequency of 10 Hz, a width of 5−7 ns, up to 10 mJ of energy, and wavelength tunable from 800 to 2000 nm. A combination of an iris, a half-wave achromatic retarder, and a polarizer was used to modulate the intensity of the idler ($I_\omega$), which was monitored with a fast-rise photodiode (Oriel 71898) and a beamsplitter. The beam was focused onto the sample with a lens of 10-mm focal length. The intensity of light scattered in the visible was measured with an end-on photomultiplier tube (Oriel 773346) with operating range 185−850 nm, gain above 5 × 10$^5$, responsivity 3.4 × 10$^4$ A/W, and rise time 15 ns. This detector received light through an assembly of a 850-nm cutoff short-pass filter (CVI), a crown-glass plano-convex lens of diameter 25.4 mm and focal length 50 mm, and an interferential filter (CVI) centered at the wavelength of interest. Filters for 450, 500, 532, 600, 650, 700, and 750 nm, with a nominal 10-nm fwhm spectral band, were used in the present study. The photomultiplier tube (PMT) was normally operated under a 1000-V bias provided by a regulated power supply (Oriel 70705); the PMT output was delivered to a 350-MHz voltage amplifier (Oriel 70723). The responses of the two detectors were independently calibrated with a power meter (Melles Griot 13PEM001). The response of each detector was kept within its calibration range by means of neutral density filters (CVI) and measured with a boxcar integrator (Stanford Research 250) whose output was acquired with a digital oscilloscope card (National Instruments NI 5112 PCI) installed in a PC and controlled with a custom LabView Virtual

Instrument. To minimize the effect of background scattered light, a foam board shielding case was built around the photomultiplier assembly and the sample mount.

For solid samples, the coefficient $d_{eff}$ was evaluated by an adaptation of the Kurtz−Perry method[11] using 7-mm diameter pellets hand-pressed in a stainless steel die from freshly ground and sieved crystals. The averaged intensity of the signal ($I_{2\omega}$) was fitted to

$$I_{2\omega} = K d_{\text{eff}}^{\ 2} I_{\omega}^{\ 2} \quad (1)$$

where $I_\omega$ is the averaged intensity of the pump measured at the reference photodiode and $d_{eff} = {}^1/_2\chi^{(2)}$. The calibration factor, $K$, was determined with standard samples of KDP and $LiNbO_3$. The value of $d_{eff}$ was further corrected for absorption using the diffuse-reflectance spectrum measured with a photodiode array spectrophotometer (Ocean Optics SD 2000), a 2800-K tungsten−halogen lamp, and a set of optical fibers and collimating lenses.

For samples in solution, the orientational average of the first hyperpolarizability was determined by hyper-Rayleigh scattering. Solutions of known concentration were filtered through a 1-$\mu$m nylon membrane (Pall Gelman) into cylindrical glass cuvettes (∅ 14.5 × 45 mm). The averaged intensity of the signal ($I_{2\omega}$) was fitted to

$$I_{2\omega} = G \Sigma N_i \langle\beta\rangle^2 I_{\omega}^{\ 2} \quad (2)$$

For each cuvette, the calibration constant, $G$, was determined by measurements of standards of freshly recrystallized *p*-nitroaniline ($\beta = 14.8 \times 10^{-30}$ esu).[48] On the basis of the absorbance spectra acquired with the photodiode array spectrometer, the factor usually employed to correct for absorption ($10^{-\text{absorbance}}$) was deemed unnecessary.

**Computational Methods.** All density functional theory calculations described here were performed with the ADF package version 2004.01.[49−51] The calculation of model geometries was based on the structures derived by crystallographic determinations; only the positions of hydrogen atoms were optimized. The optimization was gradient corrected with the exchange and correlation functionals of Perdew and Wang (PW91);[52] all basis functions had triple-$\zeta$ quality and were composed of uncontracted Slater-type orbitals (STOs), including all core electrons and two auxiliary sets of STOs for polarization. Calculations of electronic transitions used the time-dependent extension of density functional theory (TD-DFT) implemented[53−57] in the ADF package; the adiabatic local density approximation was used for the exchange-correlation kernel,[58,59] and the differentiated static LDA expression was used with the Vosko−Wilk−Nusair parametrization.[60] For the exchange-correlation potentials in the zeroth-order KS equations, the statistical average of different model potentials for occupied KS orbitals[61,62] was used. Excitation energies and oscillator strengths were obtained for the first 20 transitions using the iterative Davidson method.

## Results and Discussion

**Synthesis.** *N-n*-Butyl-4-nitroaniline (**1**) is a known compound and was prepared by reaction of 4-fluoronitrobenzene with butylamine as published;[43] crystals of this compound were grown from an acetone solution. *N-tert*-Butyl-4-nitrosulfenamide (**2**), a new species, was prepared by a modification of Miura's procedure[12−15] for thioaminyl-radical precursors. The reaction of 4-nitrophenylsufenyl chloride with primary *tert*-butylamine produced two sulfenamides 4-$NO_2C_6H_4$S-N(H)C$(CH_3)_3$ (**2**) and (4-$NO_2C_6H_4S)_2$-NC$(CH_3)_3$ (**3**). To minimize the formation of the undesired byproduct **3**, the sulfenyl halide was slowly added to an excess of the amine at ambient temperature. The product was purified by chromatography on silica gel with a base added to the eluent in order to prevent degradation on the adsorbent.

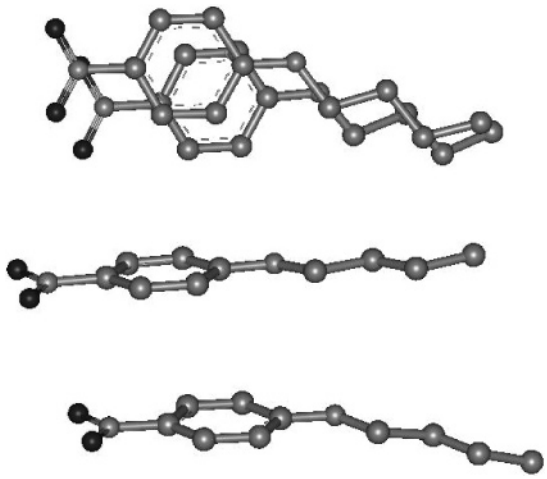

**Figure 1.** Two views of the dimers formed by $\pi$-stacking in the crystal structure of **1**.[63]

**Crystal Structures.** The structure of **1** was reported originally by Gangopaday;[63] the discussion presented here is based on the data deposited in the Cambridge Crystallographic Database.[47] In the context of the present investigations, the most prominent features of the structure are the packing in the $P2_12_12_1$ space group (point group $D_2$ or 222) and the arrangement of molecules in $\pi$-stacked dimers. The space group is non-centrosymmetric but not polar; in this situation, the components of the molecular dipole moments cancel each other and only the octupolar components of the second-order tensor contribute to the macroscopic nonlinear response. Within a dimer (Figure 1), the molecular dipoles are almost parallel (deviation 2.9°) but the angle between the aromatic rings is 5.3° and the rings are shifted with respect to each other. The closest intermolecular contacts are one N−O (3.37 Å), and two C−C (3.48 and 3.54 Å). The $\pi$-stacked dimer constitutes effectively the unit that builds the lattice. The angles between the charge-transfer axes of equivalent dimers (173.9°, 128.2°, and 52.2°) deviate significantly from the optimal orientation for second harmonic generation (109.5°) in this point group.[32]

The crystal structure of **2** was determined in the course of these investigations and is depicted in Figure 2. The molecule of compound **2** is essentially identical in bond lengths to that of 4-$CH_3C_6H_4$S-N(H)C$(CH_3)_3$[64] as well as in the torsion angle C(1)−S(1)−N(1)−C(7), 113.6(2)°, which defines a gauche conformation; in other sulfenamides the observed values range from 84.1 to 122.4°.[13] The aromatic ring is coplanar with the S−N bond and the $NO_2$ group; the deviations from the phenyl ring least-squares plane ($\chi^2 = 13.2$) are N(1) 0.062(2)°, S(1) 0.064(1)°, N(2) 0.016(2)°, O(1) 0.006(2)°, and O(2) 0.030(2)°. This is consistent with strong delocalization of sulfur electrons into the ring. The three different substituents render the nitrogen atom chiral in the solid state. The unit cell is non-centrosymmetric and belongs to the *Fdd*2 space group (point group $C_{2v}$ or *mm*2) and has a nonzero total dipole moment in the direction of **c**. Each molecule is connected to its enantiomer by a hydrogen bridge between N(1) and O(1) at $-x + {}^3/_4, y + {}^1/_4, z + {}^3/_4$. The head-to-tail interaction is repeated continuously to form an infinite chain. Parallel chains are organized in layers parallel to the (1,0,0) plane, and the aromatic rings are rotated 40° from the layer plane. The next layer consists of chains oriented at an

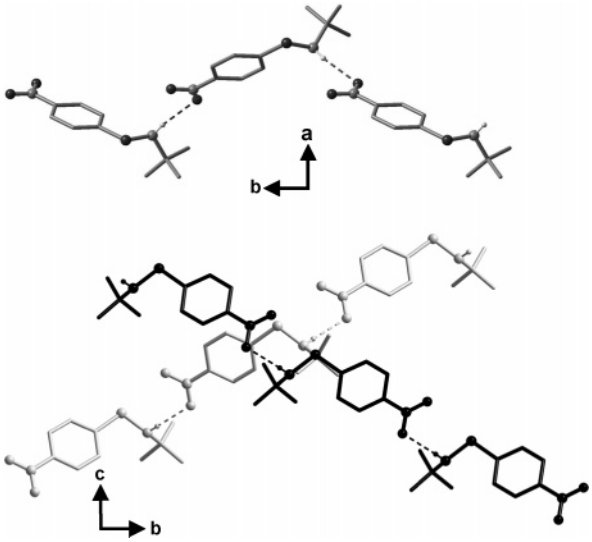


**Figure 2.** Two views of the orientation of the supramolecular chains in the crystal structure of **2**.

angle of 120°, far from the parallel orientation that is optimal in *mm*2.[32] The third layer repeats the orientation of the first, albeit the molecules are displaced along **b** and **c** relative to the first layer; the lattice is assembled by layers alternated in this way. The aromatic rings are staggered so that there is no $\pi$-stacking in the lattice.

From the point groups of these lattices, it can be readily predicted that solid **1** will be much less efficient than crystalline **2** for second harmonic generation. The orientation of the individual tensors, however, is not the only factor to consider: formation of parallel $\pi$-stacked dimers leads to a strong mutual polarization of the chromophores. This can be readily assessed by the decrease of the overall dipole moment. DFT calculations provided a dipole moment of 8.99 D for a single molecule of **1** and 17.12 D for the dimer $\mathbf{1}_2$.

**Molecular Nonlinear Optical Response.** Comparing the resonant contributions to the nonlinear response of solid **1** and **2** would only be appropriate if the molecular nonlinear responses are similar. Although nitroanailines have been exhaustively studied, there are no nonlinear data reported for any sulfenamides; it is therefore necessary to compare experimentally the molecular response of compounds **1** and **2**. The orientational averages of the first molecular hyperpolarizabilities, $\langle\beta\rangle$, were determined by hyper-Rayleigh scattering at 532 nm for samples in acetone solution. Although the molecular nonlinear optical response can be influenced by hydrogen bonding and the polarity of the solvent, these effects should be small and would not cause a large change of molecular response with respect to the solid. For the nitroaniline **1**, $\langle\beta\rangle$ was found to be $(20 \pm 2) \times 10^{-30}$ esu, and for the nitrosulfenamide it was $(9.1 \pm 0.9) \times 10^{-30}$ esu. Substituents that contain other sulfur atoms in low oxidation states have been used as electron-donor groups in push−pull chromophores because of the high polarizability of the element and its ability to delocalize electrons in conjugated systems. Solution measurements of $\beta$ (elect. field-induced second harmonic generation (EFISH) and HRS) of mono- and disubstituted benzenes have shown that the thiol (−SH), alkylsufide (−SR), thiolato (−S−), and disulfide (−S−S−R) groups are effective electron donors, although not as efficient as the dialkylamino ($-NR_2$) functionality.[8,65−67] Studies of the quadratic hyperpolarizability of 4-amino-4′-nitrodiphenyl chalcogeno-ethers by EFISH showed that the S, Se, and Te ethers have similar hyperpolarizabilities, higher than that of the O analogue.[68,69] The result indicates that the molecular nonlinear responses of

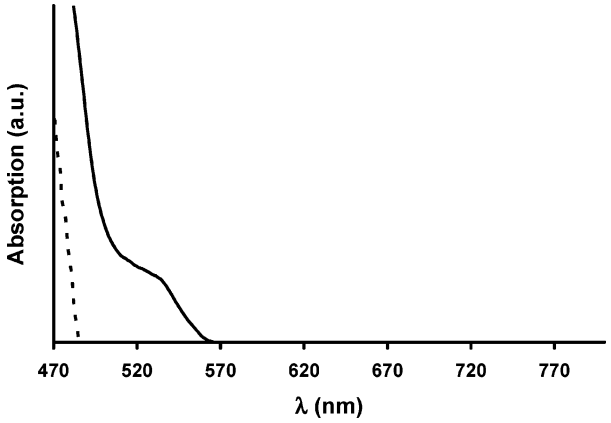


**Figure 3.** Absorption spectra of **1** (—) and **2** (- - -) in the solid state obtained from diffuse reflectance measurements.

**1** and **2** are indeed similar and it is reasonable to compare the resonant responses of the solids.

**Calculated Optical Excitations.** The hyperpolarizability is a peaked function of the optical frequency (and the wavelength) in which the peaks correspond to the resonant excitations. The simplest model to account for the dependency on the frequency is the two-level equation

$$\beta(2\omega,\omega,\omega) = \frac{{\omega_{eg}}^4}{({\omega_{eg}}^2 - 4\omega^2)({\omega_{eg}}^2 - \omega^2)}\beta_0 \qquad (3)$$

Although this approximation neglects the existence of more than one excited state, it describes reasonably well off-resonance behavior. Indeed, most $\beta$ and $d_{eff}$ measurements in the literature have been conducted at single wavelengths; the corresponding static coefficients are usually estimated by applying this model with values of excitation frequency ($\omega_{eg}$) derived from the UV−vis absorbance spectra in solution. In the present case, it would not suffice to extract the $\omega_{eg}$ from spectral data of these compounds dissolved in polar solvents because of two important considerations: First, hydrogen bond formation and other solvatochromic effects are likely to complicate the interpretation. Second, solvation is enough to dissociate the $\pi$-stacked dimers of **1**. Instead, the electronic excitations of these compounds were calculated using TD-DFT. While the first electronic excitation for the molecule of **1** (the intramolecular charge transfer) was predicted to occur at 3.3 eV, the equivalent transition for **2** was calculated to occur at 3.0 eV. The smaller excitation energy suggests that of **2** should exhibit a stronger resonant contribution; this would be reflected on a stronger wavelength dependency of the nonlinear response. The diffuse reflectance spectrum of solid **1**, however, displayed a shoulder at very long wavelength (Figure 3); this was explained with a calculation for the spectrum of dimer $\mathbf{1}_2$. The quantum mechanical method predicted the occurrence of low-energy transitions at 2.4 and 2.7 eV which are in excellent agreement with the observed shoulder at 520 nm and correspond to the excitations from the HOMO of one molecule to the LUMO of the other; the red shift of these transitions is caused by the Pauli repulsion between the aromatic rings. In contrast, the spectrum of **2** did not display any significant absorption into the visible, and a calculation for two molecules oriented as observed in the crystal structure was consistent with the observation.

**SHG from the Solids.** The second-order nonlinear optical response of crystalline samples of **1** and **2** was examined through measurements of the SHG efficiency using the Kurtz−Perry method initially at 1064 nm against standards of $KH_2PO_4$ (KDP).

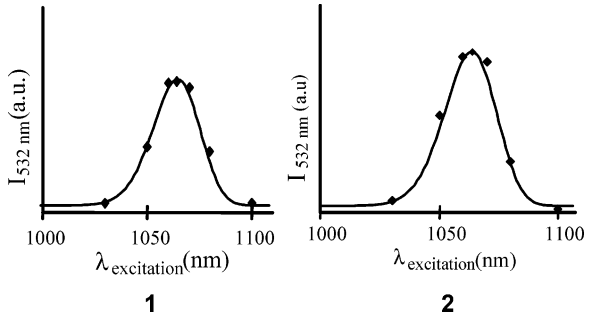


**Figure 4.** Excitation spectra of the harmonic light scattered at 532 nm by solid samples of **1** and **2**.

**TABLE 1: SHG Coefficient $d_{Eff}$ of 1 and 2 at 532 nm Relative to KDP ($d_{Eff}$ = 0.39 pm/V)**

| | particle size ($\mu$m) | |
|---|---|---|
| | 53−75 | 38−53 |
| **1** | 1.2 ± 0.1 | 1.5 ± 0.1 |
| **2** | 13 ± 1 | 12 ± 1 |

To assess the contribution of two-photon fluorescence—a common problem of organic chromophores—to the measured scattered harmonic light, the emission spectra were acquired with the photodiode array spectrometer while irradiating at 1064 nm. These consisted of single Gaussian peaks centered at 532 nm with a width of 3 nm imposed by the OPO source. However, such experiments had to be conducted at a relatively high power, which can degrade the samples and any fluorescent impurities. More sensitive measurements were conducted by monitoring the intensity of the light scattered at 532 nm while scanning the incident wavelength in the vicinity of 1064 nm. The excitation profiles acquired this way are presented in Figure 4. The experimental points follow, in both instances, Gaussian profiles with the response asymptotically decaying to the level of noise at both short and long wavelengths; the 26 nm fwhm is determined by the bandwidth of the interferential filter and the line width of the idler OPO output. Two-photon fluorescence would be distinguishable by strong emission while irradiating at the shorter wavelengths and is absent from these measurements. The final results for two particle size ranges, 53−75 and 38−53 $\mu$m, are presented in Table 1. The observations for **1** were consistent with previous studies.[63] The measurements performed for **2** were equal within experimental error for the two particle sizes, suggesting that the material is phase matchable. The value of $d_{eff}$ for **1** is 11.4 times that of KDP; this is similar to the efficiency of $LiNbO_3$ and was verified by comparison with an authentic sample of $LiNbO_3$. Similar SHG efficiencies have been observed in other organic crystalline materials, for example, [4-$CH_3NC_5H_4$—C(H)═C(H)—$C_6H_4N$-$(CH_3)_2$-4] [4-$SO_3C_6H_4CH_3$].[70] Since the molecular hyperpolarizabilities are similar, the different SHG efficiencies observed for solid **1** and **2** can be attributed in first instance to the orientation of the molecular dipoles in the respective crystals, as expected.

**TABLE 2: Resonant Parameters for the Nonlinear Optical Response of Compounds 1 and 2[a]**

| | **1** | **2** |
|---|---|---|
| $d_{eff0}$ (vs KDP) | 0.38 ± 0.05 | 5.6 ± 0.6 |
| $\omega_{eg}/10^{14}$ (Hz) | 7.6 ± 0.9 | 8.4 ± 0.9 |
| $\Delta E_{eg}$ (eV) | 3.1 ± 0.3 | 3.5 ± 0.3 |

[a] Standard errors are reported at the 95% level of confidence.

**Resonant Contribution.** To evaluate the resonant contribution to the nonlinear response of solids **1** and **2**, their second-harmonic generation efficiencies were examined between 450 and 700 nm (900 and 1400 nm for the fundamental). Only at the shortest wavelength was it necessary to correct the measured response for two-photon fluorescence and absorption. To apply it to these measurements, the two-level model was approximated to a linear expression by considering that $1 \gg \omega^2/\omega_{eg}^2 \gg \omega^4/\omega_{eg}^4$, thus

$$1 - 5\frac{\omega^2}{\omega_{eg}^2} = \frac{\beta_0}{\beta(2\omega,\omega,\omega)} \tag{4}$$

which can be applied to the solid-state case as

$$\frac{1}{d_{eff0}} - 5\frac{\omega^2}{d_{eff0}\omega_{eg}^2} = \frac{1}{d_{eff}(2\omega,\omega,\omega)} \tag{5}$$

This approximation permits in principle a simultaneous estimation of the static nonlinear optical coefficient and the frequency of the e ← g transition. It should be noted that, being derived from the two-level model, this method neglects the existence of more than one excited state. In this respect, the value of $\omega_{eg}$ should be taken with caution, it does not necessarily correspond to a single excitation, and it could instead be regarded as an "effective" value that nevertheless quantifies the resonant contribution.

Despite the limitations of the model and the problems inherent to the Kurtz−Perry method, the acquired data satisfied reasonably well the linear relationship within the range of wavelengths studied; the results are presented in graphically in Figure 5 and are summarized in Table 2. The steeper slope for compound **1** would suggest a stronger resonance enhancement, but an

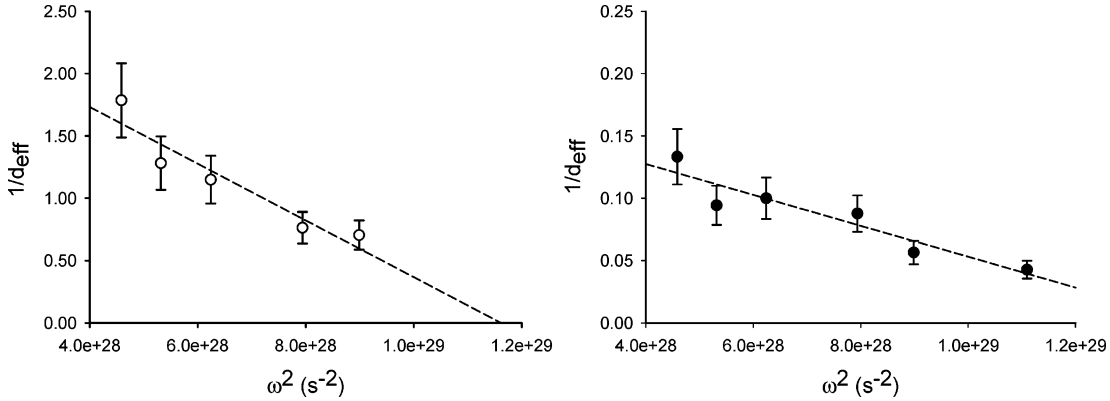


**Figure 5.** Evaluation of the resonant contribution to the nonlinear optical response of **1** (○) and **2** (●); $d_{eff}$ values are reported relative to KDP. Error bars are displayed at the 95% level of confidence.

accurate conclusion can only be obtained from the values of $\omega_{eg}$ extracted from the complete analysis. At the 95% level of confidence the numbers would be inconclusive, but at the 80% level of confidence it is possible to state that $\omega_{eg}$ is smaller, and the resonant contribution is larger, for **1** than for **2**.

## Concluding Remarks

In addition to providing a direct determination of the static nonlinear optical coefficients $d_{eff0}$, the two-level model applied to measurement of second harmonic generation efficiencies at different wavelengths provided excitation frequencies $\omega_{eg}$ that should reflect the response of molecular crystals more properly than the maxima of absorption in solution spectra. Even if the agreement is mostly qualitative, the observation of a larger resonant enhancement in the case of **1** is consistent with the new transitions enabled by intermolecular interactions in the solid. This result suggests that it is necessary to consider the effect of supramolecular $\pi$-stacking interactions in the design of materials with nonlinear optical properties and invites more detailed investigations in single crystals where the components of the dielectric tensors can be separated.

**Acknowledgment.** We thank the Natural Science and Engineering Research Council of Canada (NSERC), the Canada Foundation for Innovation (CFI), and the Ontario Innovation Trust (OIT) for funding.

**Supporting Information Available:** CIF and full crystallographic data for **2** and electronic transitions calculated by TD-DFT for **1** and **2**. This material is available free of charge via the Internet at http://pubs.acs.org.

## References and Notes

(1) Eaton, D. F. *Science* **1991**, *253*, 281−7.
(2) Andrews, D. L.; Allcock, P. *Adv. Chem. Phys.* **2001**, *119*, 603−675.
(3) Clays, K. *J. Nonlinear Opt. Phys. Mater.* **2003**, *12*, 475−494.
(4) Ledoux, I.; Zyss, J. *Novel Opt. Mater. Appl.* **1997**, 1−48.
(5) Dalton, L. R.; Steier, W. H.; Robinson, B. H.; Zhang, C.; Ren, A.; Garner, S.; Chen, A. T.; Londergan, T.; Irwin, L.; Carlson, B.; Fifield, L.; Phelan, G.; Kincaid, C.; Amend, J.; Jen, A. *J. Mater. Chem.* **1999**, *9*, 1905−1920.
(6) Kuzyk, M. G., Dirk, C. W., Eds. *Characterization Techniques and Tabulations for Organic Nonlinear Optical Materials*; Optical Engineering; Marcel Dekker: New York, 1998; Vol. 60.
(7) Albert, I. D. L.; Marks, T. J.; Ratner, M. A. *J. Am. Chem. Soc.* **1997**, *119*, 6575−6582.
(8) Cheng, L. T.; Tam, W.; Stevenson, S. H.; Meredith, G. R.; Rikken, G.; Marder, S. R. *J. Phys. Chem.* **1991**, *95*, 10631−43.
(9) Kanis, D. R.; Marks, T. J.; Ratner, M. A. *Int. J. Quantum Chem.* **1992**, *43*, 61−82.
(10) Marder, S. R.; Beratan, D. N.; Cheng, L. T. *Science* **1991**, *252*, 103−106.
(11) Ledoux, I.; Zyss, J. *C. R. Phys.* **2002**, *3*, 407−427.
(12) Riant, O.; Bluet, G.; Brasselet, S.; Druze, N.; Ledoux, I.; Lefloch, F.; Skibniewski, A.; Zyss, J. *Mol. Cryst. Liq. Cryst. Sci. Technol., Sect. A* **1998**, *322*, 35−42.
(13) Lee, Y.-K.; Jeon, S.-J.; Cho, M. *J. Am. Chem. Soc.* **1998**, *120*, 10921−10927.
(14) Brunel, J.; Ledoux, I.; Zyss, J.; Blanchard-Desce, M. *Chem. Commun.* **2001**, 923−924.
(15) Cho, M.; An, S.-Y.; Lee, H.; Ledoux, I.; Zyss, J. *J. Chem. Phys.* **2002**, *116*, 9165−9173.
(16) Goovaerts, E.; Wenseleers, W. E.; Garcia, M. H.; Cross, G. H. *Handb. Adv. Electron. Photonic Mater. Devices* **2001**, *9*, 127−191.
(17) Batten, S. R. *Curr. Opin. Solid State Mater. Sci.* **2001**, *5*, 107−114.
(18) Marder, S. R. *Inorg. Mater.* **1992**, 115−64.
(19) Le Bozec, H.; Le Bouder, T.; Maury, O.; Ledoux, I.; Zyss, J. *J. Opt. A: Pure Appl. Opt.* **2002**, *4*, S189−S196.
(20) Long, N. J. *Optoelectron. Prop. Inorg. Comput.* **1999**, 107−167.
(21) Tripathy, K.; Moreno, J. P.; Kuzyk, M. G.; Coe, B. J.; Clays, K.; Kelley, A. M. *J. Chem. Phys.* **2004**, *121*, 7932−7945.
(22) Kuzyk, M. G. *Phys. Rev. Lett.* **2000**, *85*, 1218.
(23) Kuzyk, M. G. *Phys. Rev. Lett.* **2003**, *90*, 039902.
(24) Clays, K. *Opt. Lett.* **2001**, *26*, 1699−1701.
(25) Chen, Q.; Kuang, L.; Wang, Z. Y.; Sargent, E. H. *Nano Lett.* **2004**, *4*, 1673−1675.
(26) Kanis, D. R.; Ratner, M. A.; Marks, T. J. *Chem. Rev.* **1994**, *94*, 195−242.
(27) Ma, H.; Jen, A. K. Y. *Adv. Mater.* **2001**, *13*, 1201−1205.
(28) Clays, K.; Hendrickx, E.; Verbiest, T.; Persoons, A. *Adv. Mater.* **1998**, *10*, 643−655.
(29) Persoons, A.; Verbiest, T.; Van Elshocht, S.; Kauranen, M. *ACS Symp. Ser.* **2002**, *810*, 145−156.
(30) Gubler, U.; Bosshard, C. *Nat. Mater.* **2002**, *1*, 209−210.
(31) Kauranen, M.; Verbiest, T.; Persoons, A. *J. Nonlinear Opt. Phys. Mater.* **1999**, *8*, 171−189.
(32) Zyss, J.; Oudar, J. L. *Phys. Rev. A* **1982**, *26*, 2028−48.
(33) Oudar, J. L.; Zyss, J. *Phys. Rev. A* **1982**, *26*, 2016−27.
(34) Blanchard-Desce, M.; Marder, S. R.; Barzoukas, M. *Comput. Supramol. Chem.* **1996**, *10*, 833−863.
(35) Kuzyk, M. G. In *Characterization Techniques and Tabulations for Organic Nonlinear Optical Material*; Dirk, C. W., Ed.; Optical Engineering; Marcel Dekker: New York, 1998; Vol. 60, pp 111−220.
(36) Dalton, L. R.; Harper, A. W.; Robinson, B. H. *Proc. Natl. Acad. Sci. U.S.A.* **1997**, *94*, 4842−4847.
(37) Shi, Y. Q.; Zhang, C.; Zhang, H.; Bechtel, J. H.; Dalton, L. R.; Robinson, B. H.; Steier, W. H. *Science* **2000**, *288*, 119−122.
(38) Huyskens, F. L.; Huyskens, P. L.; Persoons, A. *J. Mol. Struct.* **1998**, *448*, 161−170.
(39) Huyskens, F. L.; Huyskens, P. L.; Persoons, A. P. *J. Chem. Phys.* **1998**, *108*, 8161−8171.
(40) Steed, J. W.; Atwood, J. L. *Supramolecular Chemistry*; Wiley: New York, 2000.
(41) Bartholomew, G. P.; Ledoux, I.; Mukamel, S.; Bazan, G. C.; Zyss, J. *J. Am. Chem. Soc.* **2002**, *124*, 13480−13485.
(42) Zyss, J.; Ledoux, I.; Volkov, S.; Chernyak, V.; Mukamel, S.; Bartholomew, G. P.; Bazan, G. C. *J. Am. Chem. Soc.* **2000**, *122*, 11956−11962.
(43) Smith, H. E.; Cozart, W. I.; De Paulis, T.; Chen, F.-M. *J. Am. Chem. Soc.* **1979**, *101*, 5186−93.
(44) *AXS SMART & SAINT: Area Detector Control and Integration Software*; Bruker: Madison, WI, 1995.
(45) Sheldrick, G. M. *SADABS: Program for Empirical Absorption Correction of Area Detectors*; Bruker: Madison WI, 1996.
(46) *AXS SHELXTL*, 5.10 ed.; Bruker: Madison, WI, 1997.
(47) Allen, F. H.; Kennard, O. *Chem. Des. Autom. News* **1993**, *8*, 31.
(48) Hubbard, S. F.; Petschek, R. G.; Singer, K. D. *Opt. Lett.* **1996**, *21*, 1774−1776.
(49) Te Velde, G.; Bickelhaupt, F. M.; Baerends, E. J.; Fonseca Guerra, C.; Van Gisbergen, S. J. A.; Snijders, J. G.; Ziegler, T. *J. Comput. Chem.* **2001**, *22*, 931−967.
(50) Guerra, C. F.; Snijders, J. G.; Velde, G. T.; Baerends, E. J. *Theor. Chem. Acc.* **1998**, *99*, 391.
(51) Baerends, E. J.; Autschbach, J.; Bérces, A.; Bo, C.; Boerrigter, P. M.; Cavallo, L.; Chong, D. P.; Deng, L.; Dickson, R. M.; Ellis, D. E.; Fan, L.; Fischer, T. H.; Guerra, C. F.; Gisbergen, S. J. A. v.; Groeneveld, J. A.; Gritsenko, O. V.; Grüning, M.; Harris, F. E.; Hoek, P. v. d.; Jacobsen, H.; Kessel, G. v.; Kootstra, F.; Lenthe, E. v.; McCormack, D. A.; Osinga, V. P.; Patchkovskii, S.; Philipsen, P. H. T.; Post, D.; Pye, C. C.; Ravenek, W.; Ros, P.; Schipper, P. R. T.; Schreckenbach, H. G.; Snijders, J. G.; Sola, M.; Swart, M.; Swerhone, D.; Velde, G. t.; Vernooijs, P.; Versluis, L.; Visser, O.; Wezenbeek, E. v.; Wiesenekker, G.; Wolff, S. K.; Woo, T. K.; Ziegler, T. *ADF 2004.01 SCM, Theoretical Chemistry*; Vrije Universiteit: Amsterdam, The Netherlands, http://www.scm.com.
(52) Perdew, J. P.; Chevary, J. A.; Vosko, S. H.; Jackson, K. A.; Pederson, M. R.; Singh, D. J.; Fiolhais, C. *Phys. Rev. B* **1992**, *46*, 6671−6687.
(53) Gross, E. K. U.; Dobson, J. F.; Petersilka, M. *Top. Curr. Chem.* **1996**, *181*, 81−172.
(54) Gross, E. K. U.; Kohn, W. *Adv. Quantum Chem.* **1990**, *21*, 255−91.
(55) Gross, E. K. U.; Ullrich, C. A.; Gossmann, U. J. *NATO ASI Ser. B* **1995**, *337*, 149−71.
(56) van Gisbergen, S. J. A.; Snijders, J. G.; Baerends, E. J. *J. Chem. Phys.* **1995**, *103*, 9347−54.
(57) van Gisbergen, S. J. A.; Snijders, J. G.; Baerends, E. J. *Comput. Phys. Commun.* **1999**, *118*, 119−138.
(58) van Gisbergen, S. J. A.; Snijders, J. G.; Baerends, E. J. *Phys. Rev. Lett.* **1997**, *78*, 3097−3100.
(59) van Gisbergen, S. J. A.; Snijders, J. G.; Baerends, E. J. *J. Chem. Phys.* **1998**, *109*, 10644−10656.
(60) Vosko, S. H.; Wilk, L.; Nusair, M. *Can. J. Phys.* **1980**, *58*, 1200−1211.

(61) Gritsenko, O. V.; Schipper, P. R. T.; Baerends, E. J. *Chem. Phys. Lett.* **1999**, *302*, 199−207.
(62) Schipper, P. R. T.; Gritsenko, O. V.; van Gisbergen, S. J. A.; Baerends, E. J. *J. Chem. Phys.* **2000**, *112*, 1344−1352.
(63) Gangopadhyay, P.; Rao, S. V.; Rao, D. N.; Radhakrishnan, T. P. *J. Mater. Chem.* **1999**, *9*, 1699−1705.
(64) Mahmoudkhani, A. H.; Vargas-Baca, I. *Acta Crystallogr. E* **2003**, *59*, O1082−O1083.
(65) Abdel-Halim, H.; Cowan, D. O.; Robinson, D. W.; Wiygul, F. M.; Kimura, M. *J. Phys. Chem.* **1986**, *90*, 5654−8.
(66) Sudharsanam, R.; Chandrasekaran, S.; Das, P. K. *J. Mater. Chem.* **2002**, *12*, 2904−2908.
(67) Sylla, M.; Giffard, M.; Boucher, V.; Illien, B.; Mercier, N.; Phu, X. N. *Synth. Met.* **1999**, *102*, 1548−1549.
(68) Robinson, D. W.; Abdel-Halim, H.; Inoue, S.; Kimura, M.; Cowan, D. O. *J. Chem. Phys.* **1989**, *90*, 3427−9.
(69) Zhao, B.; Chen, C.; Zhou, Z.; Cao, Y.; Li, M. *J. Mater. Chem.* **2000**, *10*, 1581−1584.
(70) Marder, S. R.; Perry, J. W.; Yakymyshyn, C. P. *Chem. Mater.* **1994**, *6*, 1137−1147.